# Evidence of Light Guiding in Ion-Implanted Diamond

S. Lagomarsino*
*Department of Energetics University of Firenze and INFN, Via S.Marta 3, 50136 Italy*

P. Olivero and F. Bosia
*Experimental Physics Department and Nanostructured Interfaces and Surfaces Centre of Excellence, University of Torino and INFN, via P. Giuria 1, 10125 Torino, Italy*

M. Vannoni
*CNR, Istituto Nazionale di Ottica (INO), Largo E. Fermi 6, 50125 Arcetri, Firenze, Italy*

S. Calusi, L. Giuntini, and M. Massi
*Physics Department and INFN Sezione di Firenze, University of Firenze, via Sansone 1, 50019 Sesto Fiorentino, Firenze, Italy*
(Received 12 August 2010; revised manuscript received 5 November 2010; published 1 December 2010)

We demonstrate the feasibility of fabricating light-waveguiding microstructures in bulk single-crystal diamond by means of direct ion implantation with a scanning microbeam, resulting in the modulation of the refractive index of the ion-beam damaged crystal. Direct evidence of waveguiding through such buried microchannels is obtained with a phase-shift micro-interferometric method allowing the study of the multimodal structure of the propagating electromagnetic field. The possibility of defining optical and photonic structures by direct ion writing opens a range of new possibilities in the design of quantum-optical devices in bulk single-crystal diamond.

DOI: 10.1103/PhysRevLett.105.233903 PACS numbers: 42.82.Bq, 42.82.Cr, 42.87.Bg, 81.05.ug

In the last decade single color centers in diamond have attracted an ever-growing scientific interest as a very promising platform for the implementation of hybrid optical–solid-state architectures for quantum information processing, due to their unique properties such as high quantum efficiency and coherence times, photostability and, most remarkably, the possibility of operating at room temperature [1–3]. Several luminescent centers based on different defects and/or impurities in the diamond lattice have been identified, with great potential in the fields of single-photon sources and quantum cryptography [4]. As a direct consequence, a significant effort is being devoted to optimize the fabrication of optical structures to integrate single color centers in scalable devices. Different architectures are under development, ranging from the fabrication of all-diamond structures in monocrystalline [5–10], polycrystalline [11], or nanocrystalline [12,13] substrates, to the interfacing of diamond color centers to hybrid devices [14–16]. The above-mentioned all-diamond architectures rely on the fabrication of waveguides and cavities based on the refractive index contrast between diamond and air; the air-diamond interface is defined by different microfabrication and nanofabrication strategies, based on the lift-off process [5], focused ion-beam (FIB) milling [10,11], or alternatively, optical [6,7] or electron-beam [8,9] lithography combined with reactive ion etching. In comparison, direct ion microbeam writing [17], a technique extensively employed in a range of materials including polymers [18] and glasses [19] to modulate the refractive index with high accuracy and spatial control via ion-induced damage, could offer unique opportunities for a more flexible and versatile design of micro-optical and photonic devices in diamond.

In this Letter we report about the fabrication of light-waveguiding microstructures in bulk single-crystal diamond by means of direct ion writing with a scanning 3 MeV proton microbeam. This determines a local modification of the optical properties of diamond, as a small modulation of the refractive index is induced in the bulk material in subsuperficial channels. We exploited our previous extensive work on the optical modifications induced in diamond by 3 MeV proton irradiation [20], to obtain controlled increments of the refractive index in rectilinear, 500 $\mu$m-long, 12 $\mu$m-wide structures below the diamond surface, down to a depth of about 50 $\mu$m below the sample surface. In previous works on the ion-beam fabrication of buried waveguides, laser coupling and optical micro-imaging were exploited to indirectly calculate the variations in the refractive index in target materials [19,21]. Here we present a different and innovative approach: the profile of the mode amplitude is directly measured with a phase-shift micro-interferometric technique, whose results are compared with the predictions of our finite element numerical models based on the ion-induced damage profile. We employed a $3.0 \times 3.0 \times 0.5$ mm$^3$ IIa single-crystal diamond. All its faces were cut along the $\langle 100 \rangle$ directions, and three adjacent sides were optically polished down to a roughness of a few nanometers. The sample was then implanted at the external scanning microbeam facility of the LABEC laboratory in Firenze [22]. After focusing to

an approximately Gaussian spot of 12 $\mu$m width, the ion beam perpendicularly hit the polished lateral side of the sample, as shown schematically in Fig. 1, and was scanned along a rectilinear path perpendicular to the two large polished faces. The channels were implanted at fluences of $2 \times 10^{16}$, $1 \times 10^{16}$, $5 \times 10^{15}$ cm$^{-2}$, with an estimated uncertainty not exceeding 5%. The resulting vacancy density distribution, as calculated using SRIM Monte Carlo simulations [23], follows the characteristic distribution shown in Ref. [20] and recalled in Fig. 1 (left panel), peaked at a depth of approximately 50 $\mu$m. The implanted structures were then characterized with a laser interferometric microscope along the longitudinal direction of the guide. This setup was designed to characterize refractive index variations with a measurement of the phase shift of the probe laser beam induced by thin planar structures, in order to perform optical path difference measurements. Here we demonstrate that it can be successfully employed for a different kind of measurement, since the phase information of the field emerging from the narrow, long structures implanted in diamond can yield significant information about the amplitude of the waveguided modes. This modality of measurement and interpretation of the phase maps is entirely original, so that it is useful to summarize the measurement principle in relation to our purposes. As shown schematically in Fig. 2, a 632.8 nm He-Ne laser beam ($S$) is focused on a diffusion disk ($D$) by the lens ($L_1$) to define a spatially incoherent, $s$-polarized light source that is focused again by the lens ($L_2$), through a polarizing beam splitter (BS), on the back focus of a microscope objective ($O$); then the collimated beam enters the quarter wave plate ($Q$), whose back surface reflects about 10% of the incident beam intensity; the reflected beam acts as a reference wave front. The microscope objective focuses the light to cross through the sample, reflecting from a high quality mirror ($M$) back through the sample and the quarter wave plate ($Q$). Thus, on the charge-injected-device camera sensor (CID), two field contributions are superimposed, that of the reference beam and that of the radiation emerging from the front plane $\Pi$ of the sample (see the dot-dashed lines in Fig. 2). These, both being $p$ polarized, are selected by the BS, in a way that excludes any spurious reflection. A piezo-electric micro-actuator performs a relative displacement of both the mirror and the sample (block B in Fig. 2) with $\lambda_{\text{He-Ne}}/8$ steps, taking at least five consecutive intensity measurements on the CID plane, and a phase-shift algorithm is used to reconstruct phase variations of the measured electric field on the plane $\Pi$ with an accuracy of about $2\pi/1000$ rad. Figure 1 (right panel) reports an image of the interference pattern produced on the CID plane. Figure 4 (left panel) represents the same areas in the false color phase-shift maps reconstructed by the acquisition system. We now show how such phase maps can be interpreted as a direct measurement of the amplitudes of the modes propagating along the waveguides. Let the electric field on the plane $\Pi$ (in a given polarization direction) be described by the real part of the function:

$$E = \mathcal{E}(x, y)e^{i[\omega t + \phi(x,y)]}. \quad (1)$$

If the structures under consideration have a cross-sectional dimension comparable to that of the radiation wavelength, then the radiation emerging from the sample will result in a principal plane-wave part plus a perturbation produced by the structures themselves. Consequently, the field on the plane $\Pi$ will be given by the sum of three contributions: a principal part given by the back radiation reflected by the mirror ($M$) ($E_0 = \mathcal{E}_0 e^{i(\omega t + \phi_0)}$), a secondary field deriving from the reflections on the surfaces of the sample

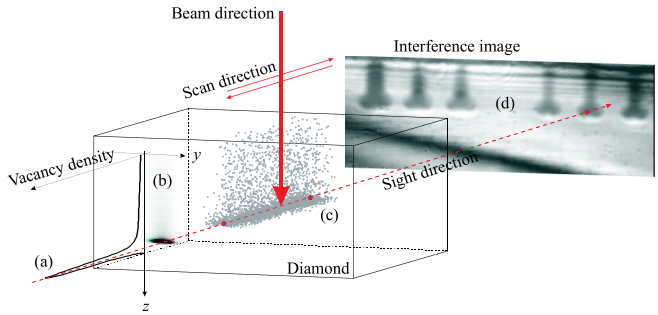


FIG. 1 (color online). Scheme of the implantation geometry. (a) Vacancy density distribution as a function of depth $z$. (b) The same distribution in a gray-scale representation, as a function of $y$ and $z$. (c) Simulation of the defect positions along the buried microchannels. (d) Interference pattern produced by the implantation.

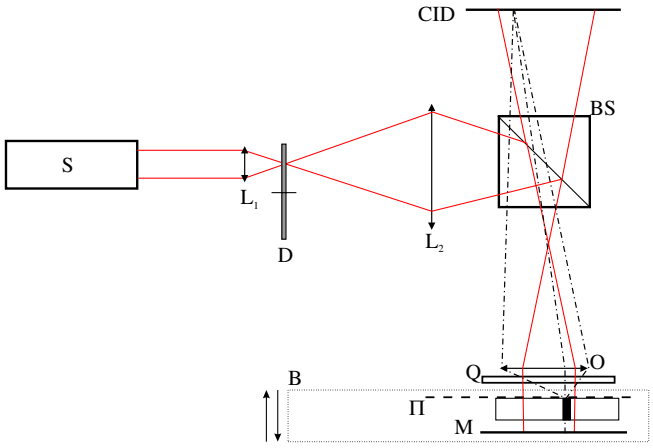


FIG. 2 (color online). Scheme of the principle of measurement of the micro-interferometer. $S$ is the laser source. $L_1$ and $L_2$ are the focalizing lenses. $D$ is the rotating diffusion disk. BS is the polarizing beam splitter. $O$ is the microscope objective. $Q$ is the quarter wave plate. $M$ is the high quality mirror. CID is the charge-injected-device camera. $\Pi$ is the plane conjugate to the CID camera plane by the objective $O$ (see the dot-dashed lines). $B$ is the block which is displaced by the micrometric actuator with respect to the rest of the apparatus.

$[E_R = \mathcal{E}_R(x, y)e^{i[\omega t+\phi_R(x,y)]}]$, and a perturbation given by the contribution to the field of the structures under consideration. If the field can be considered as guided by the structures, this contribution can be simply written as $E_G = f(x, y)e^{i(\omega t+\phi_G)}$, where the function $f(x, y)$ is the amplitude map of the mode. If $\mathcal{E}_R$ and $f$ are both small compared with $\mathcal{E}_0$, the phase difference $\Delta\phi = \phi(x, y) - \phi_0$, measured by the instrument, is given, at the lowest order, by

$$\Delta\phi = \frac{\mathcal{E}_R(x, y)}{\mathcal{E}_0}\sin(\phi_R(x, y) - \phi_0) + \frac{f(x, y)}{\mathcal{E}_0}\sin(\phi_G - \phi_0). \quad (2)$$

Consequently, once the contribution of the reflections has been fitted and subtracted, the map of $\Delta\phi$ is simply proportional to the amplitude map of one of the modes which can propagate in the structure, or to a linear combination of several modes simultaneously propagating in the waveguide, each with its appropriate phase value $\phi_G$. Thus, the reading of the maps obtained with the phase-shift method described above gives direct and promptly readable information about the amplitude of the modes propagating in the guiding structures. In order to compare the experimental phase profiles with a superposition of modes propagating in the waveguides, a two-dimensional finite element model of the irradiated regions was employed, taking into account the local modifications in the refractive index induced by proton damage, quantified in terms of the aforementioned induced vacancy density. Once the vacancy density at every cell of the simulation grid is defined, the local variation of refractive index at the He-Ne wavelength is calculated on the basis of the simple linear relation

$$\Delta n = (4.20 + 2.88i) \times 10^{-23}\frac{dN_{\text{vacancies}}}{dV/\text{cm}^3}, \quad (3)$$

in which the real part of the proportionality constant has been taken by Ref. [20], while the imaginary part was evaluated from microspectrometric measurements of uniformly irradiated areas as in Ref. [24], combined with a model taking into account the depth damage profile as in Ref. [20]. Finite element model simulations were carried out using the rf module of COMSOL Multiphysics. The specimen geometry was reproduced and meshed using quadrilateral elements, using Eq. (3) for the refractive index variation in the adjacent waveguides. The value used for the refractive index of unimplanted diamond was $n_0 = 2.41$. Simulations yield the effective mode index of the confined modes in the waveguides and the corresponding electric and magnetic field amplitude distributions. These data can be compared to the experimentally measured maps. In Fig. 3 a map of the vacancy density, as calculated by SRIM, together with an example set of nine different calculated propagation modes in the structures irradiated at the highest fluence are shown. At lower fluences, progressively lower refractive index modifications imply a lower number of propagating modes, whose amplitude maps present fewer and wider lobes.

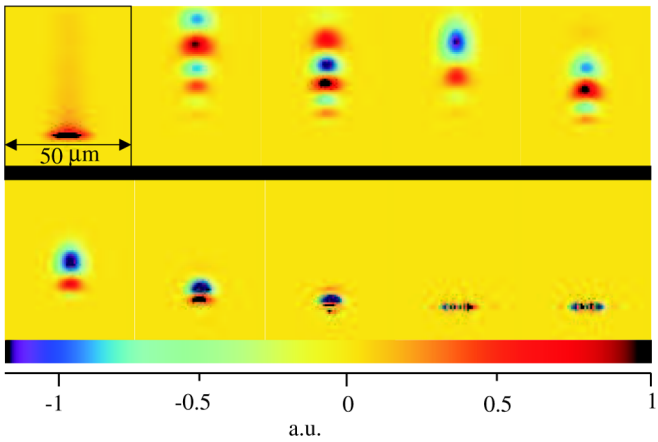


FIG. 3 (color online). (Top left) Map of the damage produced by the ion beam in terms of vacancy density. (Rest of the figure) In the same spatial scale, amplitude maps of nine simulated modes propagating in the waveguide irradiated at a fluence of $2 \times 10^{16}$ cm$^{-2}$.

The experimentally obtained, two-dimensional phase maps were compared with the calculated amplitude maps, by fitting them with a linear combination of the propagating modes, via a least-square error algorithm.

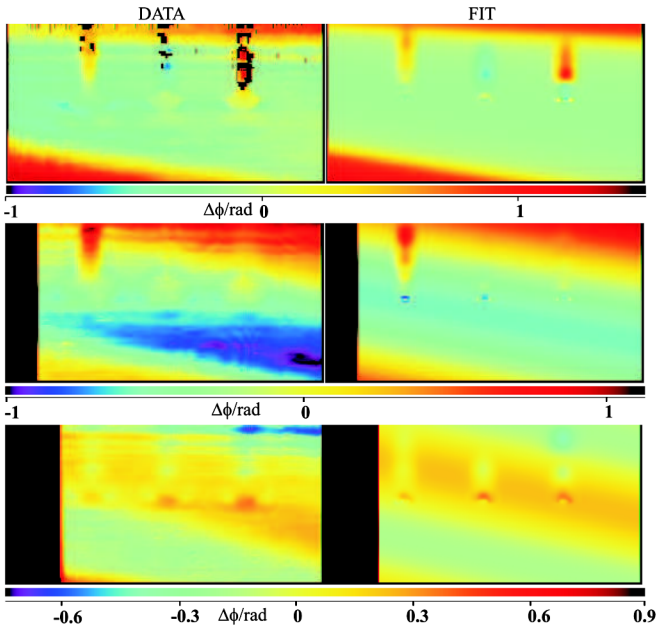


FIG. 4 (color online). Comparison between the measured phase-shift maps (left panels) and the fit (right panels) obtained by a linear superposition of mode amplitudes and a background, taking into account multiple reflections effects. (Top and middle panels) Images related to three adjacent guides obtained with irradiation at $2 \times 10^{16}$ cm$^{-2}$ (left) and at $1 \times 10^{16}$ cm$^{-2}$ (middle and right). (Bottom) Images related to three guides irradiated at the fluence of $5 \times 10^{15}$ cm$^{-2}$.

Since the relative amplitudes of the modes excited in the waveguides critically depend on the illumination conditions, different positions of the sample on the focal plane may imply different weights to be assigned at each particular mode. In Fig. 3 (left side, top and middle) two different images of the same implantations at fluences of $2 \times 10^{16}$ cm$^{-2}$ and $1 \times 10^{16}$ cm$^{-2}$ are reported along with their respective best fits (on the right) obtained with 30 different propagation modes (located in groups of 10 modes on the three structures) and a combination of sinusoids to model the background given by the reflections on the two diamond plane surfaces. It is evident that the same set of propagation modes, though with different weights, fit the two images. The weight of each mode is not of much significance, since it is proportional to the sine of $(\phi_G - \phi_0)$, a phase shift which is supposed to vary randomly from one mode to another. In the same figure (bottom), an image of the waveguide implanted at a fluence of $5 \times 10^{15}$ cm$^{-2}$ is also shown, together with its 21-modes fit. From the inspection of these images we conclude that the adherence of the fit to the experimental phase profiles is very satisfactory in the cap layer between 0 and $\approx 45$ $\mu$m in depth, where the relative damage is small, while at the end of the range the structures seem to be more diffuse, probably due to the distortion induced by diffraction on the highly opaque regions, which lie under the plane $\Pi$ (see Fig. 2) in correspondence with the considered structures. In conclusion, the comparison of experimental results and numerical calculation provides evidence that the described ion-beam writing method offers the possibility to fabricate light-guiding structures in bulk diamond. Moreover, our micro-interferometric measuring method provides powerful means for a highly detailed study of the mode patterns propagating in the waveguides. This strategy to modulate the refractive index offers a vast range of fabrication possibilities in diamond-based optical devices, which go far beyond the proof-of-principle demonstration presented here, as already foreseen in theoretical papers modeling the effect of refractive index modulation on the performance of photonic-crystal cavities in diamond [25].

This work was financially supported in the framework of the INFN experiment FARE. The authors are grateful to Anna Sytchkova and Andrea Sordini for the optical characterization of the samples.

*lagomarsino@fi.infn.it

[1] P. Kok and B. W. Lovett, Nature (London) **444**, 49 (2006).
[2] S. Prawer and A. D. Greentree, Science **320**, 1601 (2008).
[3] R. F. Service, Science **329**, 616 (2010).
[4] J. O. Orwa, A. D. Greentree, I. Aharonovich, A. D. C. Alves, J. V. Donkelaar, A. Stacey, and S. Prawer, J. Lumin. **130**, 1646 (2010).
[5] B. A. Fairchild, P. Olivero, S. Rubanov, A. D. Greentree, F. Waldermann, R. A. Taylor, I. Walmsley, J. M. Smith, S. Huntington, B. C. Gibson *et al.*, Adv. Mater. **20**, 4793 (2008).
[6] M. P. Hiscocks, C. J. Kaalund, F. Ladouceur, S. T. Huntington, B. C. Gibson, S. Trpkovski, D. Simpson, E. Ampem-Lassen, S. Prawer, and J. E. Butler, Diam. Relat. Mater. **17**, 1831 (2008).
[7] M. P. Hiscocks, K. Ganesan, B. C. Gibson, S. T. Huntington, F. Ladouceur, and S. Prawer, Opt. Express **16**, 19512 (2008).
[8] T. M. Babinec, B. J. M. Hausmann, M. Khan, Y. Zhang, J. R. Maze, P. R. Hemmer, and M. Loncar, Nature Nanotech. **5**, 195 (2010).
[9] B. J. M. Hausmann, M. Khan, Y. Zhang, T. M. Babinec, K. Martinick, M. McCutcheon, P. R. Hemmer, and M. Loncar, Diam. Relat. Mater. **19**, 621 (2010).
[10] T. M. Babinec, J. T. Choy, K. J. M. Smith, M. Khan, and M. Loncar, arXiv:1008.1431v1.
[11] J. P. Hadden, J. P. Harrison, A. C. Stanley-Clarke, L. Marseglia, Y. L. D. Ho, B. R. Patton, J. L. OBrien, and J. G. Rarity, arXiv:1006.2093v1.
[12] C. F. Wang, R. Hanson, D. D. Awschalom, E. L. Hu, T. Feygelson, J. Yang, and J. E. Butler, Appl. Phys. Lett. **91**, 201112 (2007).
[13] C. F. Wang, Y.-S. Choi, J. C. Lee, E. L. Hu, J. Yang, and J. E. Butler, Appl. Phys. Lett. **90**, 081110 (2007).
[14] D. M. Toyli, C. D. Weis, G. D. Fuchs, T. Schenkel, and D. D. Awschalom, Nano Lett. **10**, 3168 (2010).
[15] T. van der Sar, J. Hagemeier, W. Pfaff, E. C. Heeres, T. H. Oosterkamp, D. Bouwmeester, and R. Hanson, arXiv:1008.4097v1.
[16] D. Englund, B. Shields, K. Rivoire, F. Hatami, J. Vukovi, H. Park, and M. D. Lukin, Nano Lett. **10**, 3922 (2010).
[17] A. Bettiol, T. Sum, F. Cheong, C. Sow, S. V. Rao, J. van Kan, E. Teo, K. Ansari, and F. Watt, Nucl. Instrum. Methods Phys. Res., Sect. B **231**, 364 (2005).
[18] T. Sum, A. Bettiol, H. Seng, I. Rajta, J. van Kan, and F. Watt, Nucl. Instrum. Methods Phys. Res., Sect. B **210**, 266 (2003).
[19] A. A. Bettiol, S. V. Rao, E. J. Teo, J. A. van Kan, and F. Watt, Appl. Phys. Lett. **88**, 171106 (2006).
[20] P. Olivero, S. Calusi, L. Giuntini, S. Lagomarsino, A. L. Giudice, M. Massi, S. Sciortino, M. Vannoni, and E. Vittone, Diam. Relat. Mater. **19**, 428 (2010).
[21] M. L. von Bibra and A. Roberts, J. Lightwave Technol. **15**, 1695 (1997).
[22] L. Giuntini, M. Massi, and S. Calusi, Nucl. Instrum. Methods Phys. Res., Sect. A **576**, 266 (2007).
[23] J. Ziegler, M. D. Ziegler, and J. Biersack, Nucl. Instrum. Methods Phys. Res., Sect. B **268**, 1818 (2010).
[24] A. K. Sytchkova, J. Bulir, and A. M. Piegari, Chin. Optic. Lett. **8**, Suppl. 1, 103 (2010).
[25] S. Tomljenovic-Hanic, A. D. Greentree, C. M. de Sterke, and S. Prawer, Opt. Express **17**, 6465 (2009).